Eur. Phys. J. A (2011) **47**: 106
DOI 10.1140/epja/i2011-11106-4

THE EUROPEAN PHYSICAL JOURNAL A

Regular Article – Experimental Physics

# Half-life measurements of $^{137,139}$Cs excited nuclear states

B. Roussière[1,a], M.A. Cardona[2,3,4], I. Deloncle[5], D. Hojman[2,4], J. Kiener[5], P. Petkov[6], D. Tonev[6], Ts. Venkova[6], and the ALTO Collaboration

[1] Institut de Physique Nucléaire, IN2P3/CNRS/Université Paris-Sud, F-91406 Orsay, France
[2] Departamento de Física, Comisión Nacional de Energía Atómica, 1429 Buenos Aires, Argentina
[3] Universidad Nacional de General San Martín, San Martín, Argentina
[4] CONICET, 1033 Buenos Aires, Argentina
[5] Centre de Spectrométrie Nucléaire et de Spectrométrie de Masse, IN2P3/CNRS/Université Paris-Sud, F-91405 Orsay, France
[6] Institute for Nuclear Research and Nuclear Energy, Bulgarian Academy of Sciences, 1784 Sofia, Bulgaria

Received: 24 January 2011 / Revised: 6 July 2011
Published online: 19 September 2011 – 
Communicated by J. Äystö

**Abstract.** A fast-timing setup has been developed to measure the nuclear-state half-lives of neutron-rich nuclei. The first on-line measurements were performed on $^{137,139}$Cs obtained from the $\beta^-$ decay of $^{137,139}$Xe. These neutron-rich Xe nuclei were produced by the $^{238}$U photofission induced by the 50 MeV electron beam delivered by the ALTO facility. The half-lives of the first excited state in $^{137}$Cs and of six excited states in $^{139}$Cs were measured for the first time. Taking into account new information given by the deduced transition probabilities, we discuss the structure of the first excited states in $^{137,139}$Cs: it is shown that, in both nuclei, the first excited $\frac{5}{2}^+$ level corresponds mainly to the one-proton state issued from the $\pi 2d_{5/2}$ orbital and that the most probable spin values for the states located at 289.8, 393.5, and 393.8 keV in $^{139}$Cs are $\frac{5}{2}^+$, $\frac{3}{2}^+$, and $\frac{1}{2}^+$, respectively.

## 1 Introduction

Half-lives of excited nuclear states, giving access to transition probabilities, provide direct insight into the structure of the nucleus and offer one of the most stringent tests of the nuclear models. The fast-timing technique is well adapted to measure half-lives in the subnanosecond range. Developed first with $BaF_2$ crystals [1], this method experiences a revival of interest due to the advent of $LaBr_3$ scintillators [2] that have good properties for nuclear spectroscopy [3,4]: high scintillation light yield, fast emission and the best energy resolution among all scintillators.

We have developed a fast-timing setup including various scintillators. For the present study of nuclei fed by $\beta^-$ decay, it consists in a plastic for $\beta$ detection, $BaF_2$ and $LaBr_3$ detectors for $\gamma$ detection. At first, we performed off-line tests with standard radioactive sources ($^{60}$Co, $^{133}$Ba and $^{152}$Eu) in order to optimize the performances of our fast-timing setup. Then we needed on-line measurements to fully characterize our experimental setup and demonstrate its ability to measure half-lives in the range from some ten picoseconds to some nanoseconds. Since the linac at the ALTO facility in Orsay, dedicated to the production of neutron-rich nuclei from photofission induced by a 50 MeV electron beam [5], had not yet received the authorization to run with full electron-beam intensity, it was only possible to carry out tests with a low-intensity electron beam. Therefore, for the first fast-timing on-line experiment, we measured the half-life of the first excited states of $^{137,139}$Cs obtained by the $\beta^-$ decay of $^{137,139}$Xe that are well produced at ALTO in spite of these restrictive working conditions. The knowledge of the excited-nuclear-state half-lives and of the deduced transition probabilities in the odd-$Z$ $^{137,139}_{55}Cs_{82,84}$ nuclei gives precious information on the proton states near the neutron closed shell $N = 82$. In particular, it is shown that, in both nuclei, the first excited $\frac{5}{2}^+$ level corresponds mainly to the one-proton state issued from the $\pi 2d_{5/2}$ orbital. The most probable spin values for the states located at 289.8, 393.5, and 393.8 keV in $^{139}$Cs appear to be $\frac{5}{2}^+$, $\frac{3}{2}^+$, and $\frac{1}{2}^+$, respectively, indicating that the $\pi 2d_{5/2}$, $\pi 2d_{3/2}$, and $\pi 3s_{1/2}$ orbitals play a major role at low energy in these nuclei.

## 2 Experimental procedure

The experiment was carried out at the ALTO facility in Orsay [5]. The 50 MeV electron beam delivered by the linac impinged on a thick uranium-carbide ($UC_x$) target

[a] e-mail: roussier@ipno.in2p3.fr

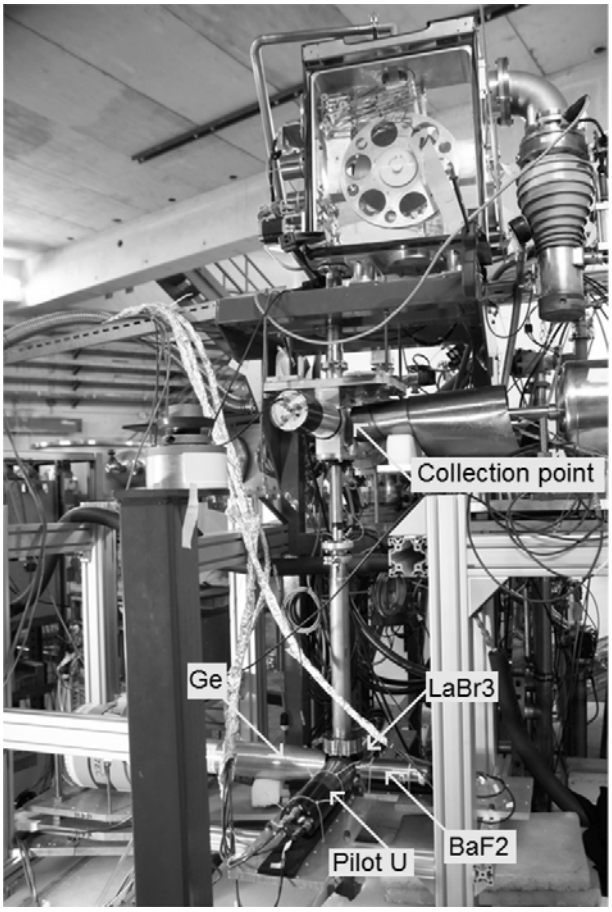


**Fig. 1.** The experimental setup used at ALTO for the fast-timing measurements.

producing bremsstrahlung radiations that induce the fission of $^{238}$U. The target, weighing 65.37 g, was composed of 122 $UC_x$ disks, 14 mm in diameter and 1 mm thick, separated by graphite fibers. It was associated with a MK5 ISOLDE-type hot plasma ion source [6]. The radioactive atoms released from the target effused into the ion source via the transfer line. The temperature of the target and of the transfer line was 2000 °C, that of the ion source 1800 °C. The produced ions were extracted under 30 kV then mass-separated by the PARRNe uniform-field H-shaped magnet with a 65° deflecting angle and a mass resolving power of 1300. The radioactive ions of the chosen mass were guided towards the measurement station where they were collected on a Mylar-aluminium tape. The collected radioactive sources were then transported in front of the detection setup (see fig. 1).

As previously mentioned, the fast-timing setup was composed of three scintillators: one Pilot U plastic for $\beta$ detection, one $BaF_2$ and one $LaBr_3$ crystals for $\gamma$ detection. All three have 25.4 mm diameters and 3, 30, and 10 mm lengths, respectively, and they are coupled to XP2020, XP2020Q, and XP20D0 photomultipliers. The thin $\beta$ detector offers a great advantage: high-energy $\beta$-rays emitted by neutron-rich nuclei with high $Q_\beta$ values deposit similar energy (around 600 keV for a 3 mm thick plastic scintillator) when passing through the detector, which provides a uniform timing response as emphasized in ref. [1]. A Ge(HP) detector was added to the setup. Its excellent energy resolution allowed the accurate selection of a decay branch by performing $\beta$-$\gamma$($BaF_2$ or $LaBr_3$)-$\gamma$(Ge(HP)) triple coincidences. The four detectors were placed around a Plexiglass tube 4 cm in diameter and 2 mm thick. Their front faces were at 2.5 cm from the radioactive source. Under these conditions, the efficiency of the $\beta$ detector was around 7% and its typical counting rate around 5000 c/s. The counting rates were around 7600, 8500 and 10500 c/s for the $BaF_2$, $LaBr_3$ and Ge(HP) detectors, respectively. With such counting rates, no problem of dead time and pile-up in the detectors is encountered. It is worth noting that electrons with energy less than 600 keV are absorbed by the Plexiglass tube, which means that most of the internal conversion electrons cannot reach the $\beta$ detector.

In order to obtain accurate and reliable results, the fast-timing method requires great care in the implementation of the experimental setup as well as in the data analysis. In the present experiment, no collimator was set at the collection point. In this case, the reproducibility of the radioactive source position depends directly on the stability of the radioactive beam. For the production of xenon nuclei, the MK5 source was used in steady conditions, applying moderate values to its parameters. The operating conditions of the ion source were very stable, and only very small fluctuations in the intensity, size and geometry of the beam could occur. On the other hand, the accuracy on the displacements performed by the tape transport system is better than 1 mm. The radioactive-beam stability was continuously checked by measuring the counting rate. When the counting-rate variations were observed to be above 15%, the measurements were stopped and the cause of these variations investigated: every time, they were found to be due to changes in intensity of the primary electron beam, and thus (since the electron-beam intensity used, $\sim$ 500 nA, was low) without any impact on the running conditions of the ion source. Therefore the variations in the radioactive-source position are expected to be slow and mainly of the order of fluctuations; they will affect the time spectra mainly by increasing their widths. Moreover, the timing electronics and the photomultiplier gains are sensitive to temperature changes. The experimental hall is well insulated from the outside by thick concrete walls and is equipped with a forced air circulation which keeps the temperature constant within $\pm$1 °C. Under these conditions, a drift of the centroid, that could reach 5 ps per hour, was observed in the time spectra; these drifts were corrected during the off-line data treatment.

The data acquisition was completed with two COMET-6X modules associated with the NARVAL system [7]. One COMET-6X module accepts up to six channels, it encodes amplitude signals and associates them with an absolute time information. However, the step of this time information is 400 ps, which is not short enough for fast-timing purpose. Therefore we have used three high-precision time-to-amplitude converters (TAC) to measure the time differences between the signals issued from the three fast detectors. If the $\beta$ detector is involved

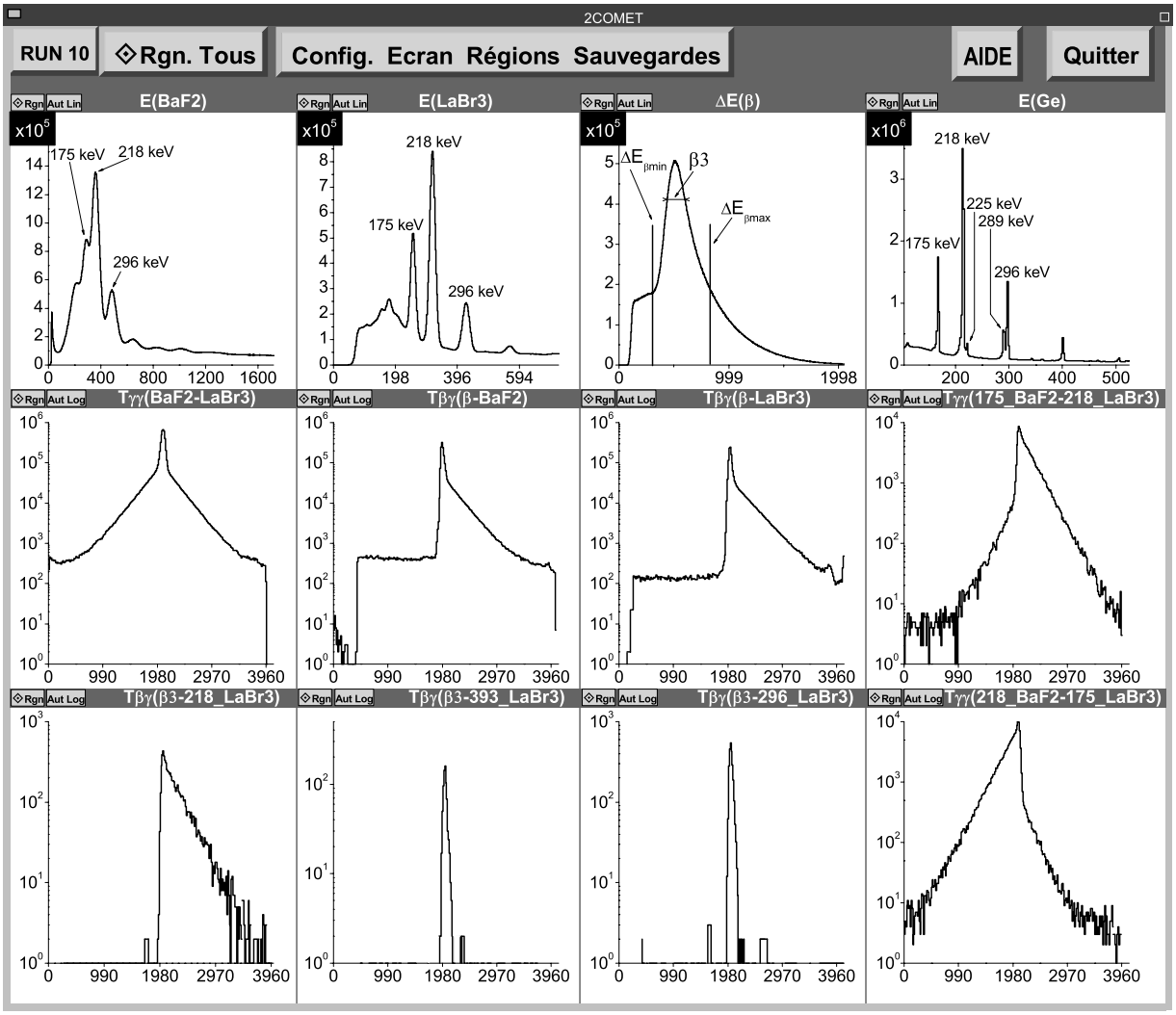


**Fig. 2.** On-line screen capture of the NARVAL acquisition spectrum window. The energy (or $\Delta E$ for $\beta$ detector) singles spectra are shown on the first row. The first three spectra displayed on the second row are the TAC singles spectra, they are marked by the name of the detectors used as start and stop signals. The other spectra are double-gated TAC spectra, they are labeled by the energy conditions required to accept the start and stop signals.

in the time measurement, it is used as the start signal for the TAC module, otherwise the start signal is provided by the $BaF_2$ detector. The full scale of the TAC modules was 50 ns. A new user C program [8] based on concepts elaborated in FANTASTIC [9] has been developed and associated with NARVAL to obtain on-line double-gated coincidence spectra from $n$-tuple (triple or more) coincident events. Figure 2 shows an on-line screen capture of the NARVAL acquisition spectrum window obtained during the $A = 139$ measurement. On the first row the three $\gamma$-energy spectra as well as the $\Delta E$ spectrum obtained with the $\beta$ detector are displayed. On the three $\gamma$ spectra, the 175, 218 and 296 keV transitions assigned to the $^{139}\mathrm{Xe} \xrightarrow{\beta^-} {}^{139}\mathrm{Cs}$ decay are indicated. In the $BaF_2$ spectrum, the 175 keV $\gamma$ line appears only as an outgrowth on the left side of the 218 keV $\gamma$ line and the 296 keV line overlaps with the tail of the 218 keV $\gamma$-ray. The much better energy resolution of the $LaBr_3$ scintillator allows a complete separation of these three peaks. With the Ge detector, not only these three peaks are well separated, but two other less intense $\gamma$-rays become visible: the first one at 225 keV on the right side of the 218 keV line and the second one at 289 keV on the left side of the 296 keV transition. The background observed in the $\gamma$-ray singles spectra arises principally from the Compton continuum. In most cases, its influence on time spectra can be neglected, in particular when the background can be eliminated by setting gates on coincident $\gamma$-ray energy in the $\gamma$ detectors. This point will be exemplified in the next section. The first three spectra shown in the second row of fig. 2 are the total TAC spectra. The last five spectra shown in fig. 2 are double-gated TAC spectra. For the $\beta$ detector, five thin slices have been defined in the $\Delta E$ spectrum: the third one, labeled $\beta 3$, corresponds to a gate centered on the maximum of the $\Delta E$ peak and was

used to build the $T_{\beta\gamma}(\beta 3\text{-}218_{\mathrm{LaBr_3}})$, $T_{\beta\gamma}(\beta 3\text{-}393_{\mathrm{LaBr_3}})$, and $T_{\beta\gamma}(\beta 3\text{-}296_{\mathrm{LaBr_3}})$ spectra shown in fig. 2. For the $BaF_2$ and $LaBr_3$ detectors, the selected energy windows correspond to the most intense transitions (175, 218, 296, 393, and 613 keV) of the $^{139}Xe \rightarrow {}^{139}Cs$ decay. From these double-gated spectra, we could see on-line that the level in $^{139}Cs$ de-exciting by the 218 keV transition has a long half-life (see the $T_{\gamma\gamma}(175_{\mathrm{BaF_2}}\text{-}218_{\mathrm{LaBr_3}})$, $T_{\beta\gamma}(\beta 3\text{-}218_{\mathrm{LaBr_3}})$, and $T_{\gamma\gamma}(218_{\mathrm{BaF_2}}\text{-}175_{\mathrm{LaBr_3}})$ spectra in fig. 2); on the contrary, the $T_{\beta\gamma}(\beta 3\text{-}393_{\mathrm{LaBr_3}})$ spectrum exhibits a narrow time distribution, which indicates a short half-life for the level decaying by the 393 keV transition.

In addition to building the control spectra, the NARVAL software sends all the events —constituted by an amplitude (energy signal from a detector or analog output from a TAC) associated with its absolute time— to be recorded on disk. Off-line, the data were sorted into several tri-dimensional coincidence matrices labeled $\mathcal{M}(E_{\mathrm{X}}\text{-}E_{\mathrm{Y}}\text{-}T_{\mathrm{X\text{-}Y}})$[1] having on the first axis the energy detected by one of the fast detectors, X, on the second axis the energy detected by another fast detector, Y, and on the third axis the signal of the TAC with X and Y detectors as start and stop. Other matrices labeled $\mathcal{M}(E_{\mathrm{X}}\text{-}E_{\mathrm{Ge}}\text{-}T_{\beta\text{-}\mathrm{X}})$, where X stands for $BaF_2$ or $LaBr_3$, were built; they allow us to take advantage of the excellent energy resolution of the Ge(HP) detector to accurately select, if necessary, a decay branch. They were obtained by keeping, among the four-dimensional coincidence events $\Delta E_\beta\text{-}E_{\mathrm{X}}\text{-}E_{\mathrm{Ge}}\text{-}T_{\beta\text{-}\mathrm{X}}$, only those with $\Delta E_\beta$ lying within two limits $\Delta E_{\beta min}$ and $\Delta E_{\beta max}$ indicated by markers in fig. 2. Then the time spectra were extracted from all these matrices by setting gates on the energy axes. If the time spectra were obtained from a $\mathcal{M}(E_\beta\text{-}E_{\mathrm{X}}\text{-}T_{\beta\text{-}\mathrm{X}})$ matrix, the above window, defined by $\Delta E_{\beta min}$ and $\Delta E_{\beta max}$, was used for the gate set on the $\beta$ detector in order to ensure the same timing response of the $\beta$ detector for all the time spectra. Finally the time spectra were analyzed either by the shape deconvolution method when the half-life of the nuclear state is long enough to show up as a slope on the delayed part of the time spectrum and/or by the centroid-shift method in the other cases. The latter method allowed the measurement of half-lives as short as 10 ps [1,10].

## 3 Experimental results

During the experiment, the $^{139}Xe$ yield was used to optimize and monitor the linac: at 500 nA of incident electron beam, $2 \times 10^5$ ions per second were measured on-line using the Ge(HP) detector. The calibration of the fast-timing setup and, to some extent, the check of the measurement and analysis procedures were performed using the $^{138}Cs \rightarrow {}^{138}Ba$ decay. The 137 and 139 mass studies allowed us to measure, for the first time, the half-lives of the first excited states of $^{137,139}Cs$. The measurement cycles were chosen in order to optimize the counting rates: the collection ($t_c$) and measuring ($t_m$) times were equal to $t_c = 7.5$ min and $t_m = 30$ min for the $A = 138$ mass study, to $t_c = t_m = 4$ min and $t_c = t_m = 40$ s for the $A = 137$ and 139 mass studies, respectively.

### 3.1 A = 138 results

With the collection and measuring times chosen for the $A = 138$ measurements, the $\gamma$ lines signing the $^{138}Cs \rightarrow {}^{138}Ba$ $\beta^-$ decay are present in the spectra.

The $^{138}Ba$ level scheme is well known and the half-lives of the states populated by the $^{138}Cs$ $\beta^-$ decay had been measured [11]. The half-lives of the levels located at 1899, 2091, 2203, and 2415 keV were determined to be: $T_{1/2} =$ 2.164 (11) ns, 0.8 (1) $\mu$s, 55 (17) ps, and 16 (8) ps, respectively. The other levels have shorter half-lives. Therefore, in view of the timing properties of the detectors used in our experiment, the transitions de-exciting these latter levels can be considered as prompt transitions and used for time calibration. The time spectra obtained by setting gates on the most intense $\gamma$-rays (*i.e.* on the 138, 409, 463, 547, 872, 1010 and 1436 keV $\gamma$ lines) were extracted from the $\mathcal{M}(E_\beta\text{-}E_{\mathrm{BaF_2}}\text{-}T_{\beta\text{-}\mathrm{BaF_2}})$, $\mathcal{M}(E_\beta\text{-}E_{\mathrm{LaBr_3}}\text{-}T_{\beta\text{-}\mathrm{LaBr_3}})$, and $\mathcal{M}(E_{\mathrm{BaF_2}}\text{-}E_{\mathrm{LaBr_3}}\text{-}T_{\mathrm{BaF_2\text{-}LaBr_3}})$ matrices. In the latter case, the time spectra were built for gates set on transitions coincident in the level scheme, namely the 138-409, 138-872, 463-1436, 1010-1436, 409-463, and 547-463 keV cascades and the inverted pairs.

The analysis of most of the time spectra has allowed us to determine the prompt-curve properties. The full width at half maximum (FWHM) was determined by fitting the time spectra considered as prompt curves using a Gaussian function. Then applying the method described in ref. [12], the intrinsic time resolution of the $BaF_2$ and $LaBr_3$ detectors was determined, as a function of the $\gamma$-ray energy, from the FWHM of the time spectra (see fig. 3). The energy dependence is found to be quite similar to that obtained off-line while investigating the time response from prompt coincidence events using the Compton and full-energy $\gamma$-rays emitted by a $^{60}Co$ source. However, it was found, as in ref. [1], that the prompt time spectra are not true Gaussian, they are narrower at the top and wider at the bottom and can exhibit some asymmetries arising from electronic adjustments (*e.g.*, the constant fraction discriminator adjustments, the high voltage setting on the phototubes), electronic time drifts and counting rates. In order to quantify these asymmetries, the prompt time spectra were fitted with the function resulting from the convolution of a Gaussian function and an exponential function $e^{-\lambda_a t}$ (with $\lambda_a = \ln(2)/T_{1/2,a}$). The $T_{1/2,a}$ parameter is not a real half-life but an apparent half-life used to describe the deviation of the experimental prompt curve from a Gaussian approximation. We found that all the prompt experimental time spectra exhibit a very similar apparent half-life, $T_{1/2,a} \sim 20$ ps. It was shown in ref. [1] that the parameter $T_{1/2,a}$ can be used to determine the lower limit for which the deconvolution method can be reliably used. Applying the criterion given in ref. [1], the following limit is obtained for the present experiment: $T_{1/2} = 60$ ps.

[1] Strictly speaking $\Delta E_\beta$ should be used for the $\beta$ detector as the scintillator used is thin, but for simplification's sake $E_\beta$ will be used in the following.

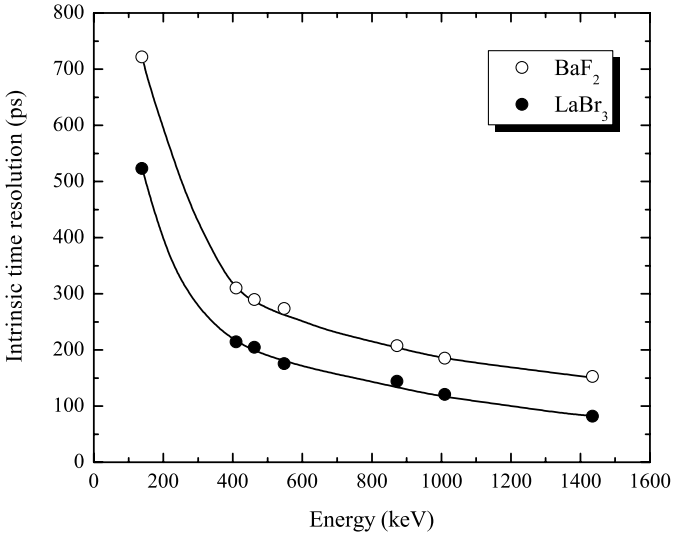


**Fig. 3.** Intrinsic time resolution of the $BaF_2$ and $LaBr_3$ detectors.

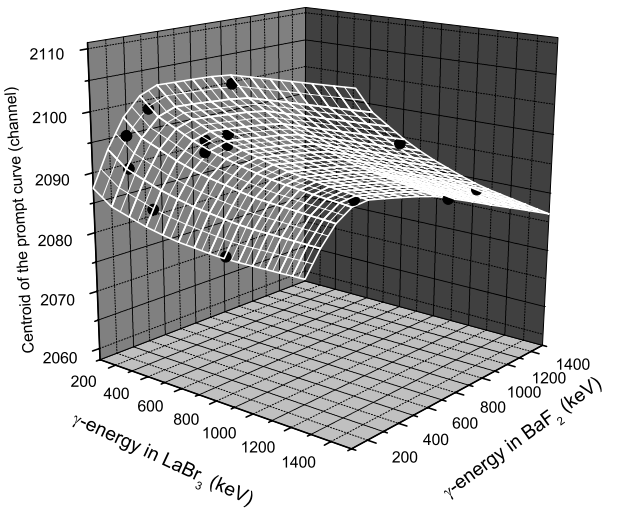


**Fig. 4.** Centroids of the prompt curve for time measurements performed between the $BaF_2$ and $LaBr_3$ detectors. The dots represent the measured values and the grid the values determined from the $\beta$-$BaF_2$ and $\beta$-$LaBr_3$ time measurements on the $A = 138$ mass.

We have also compared the position of the prompt-curve centroid as a function of the $\gamma$-ray energy for time measurements performed between the $\beta$ and $BaF_2$ or $LaBr_3$ detectors or between the $BaF_2$ and $LaBr_3$ detectors. Figure 4 shows the result obtained in the latter case: one can note the excellent agreement between the values observed experimentally (dots) and those calculated from $\beta$-$BaF_2$ and $\beta$-$LaBr_3$ time measurements (grid). This points out the consistency of our measurement and analysis procedures. It is worth noting that the centroid of the $\beta$-$\gamma$ time spectra depends slightly on the average $\beta$ energy detected and can therefore vary slightly with the radioactive decay or mass studied. This dependence has been checked for $A = 139$ by analyzing the $\beta$-$\gamma$ time spectra obtained from gates set on the $\gamma$-Compton continuum (after being sure that no transition associated with a "long" half-life contributes to this Compton background) or prompt $\gamma$-rays. The resulting prompt position curve is not very accurate, however the accuracy, at worst $\sim \pm 10$ ps below 400 keV, is sufficient to obtain by the centroid-shift method an estimate of the half-lives in the range of tens of picoseconds. For $A = 137$ this energy dependence of the centroid could not be studied because the $\gamma$ spectrum exhibits only the most intense transition from the $^{137}$Xe decay (see sect. 3.2). On the other hand, we did not find that the width of the $\beta$-$\gamma$ prompt curves was affected by these small changes in the detected $\beta$ energy between neighboring isotopes.

In the following, the experimental time spectra are fitted with the function resulting from the convolution of a prompt response (approximated by a Gaussian function) and an exponential function $e^{-\lambda t}$ (with $\lambda = \ln(2)/T_{1/2}$ the decay constant characterizing the studied excited state), the three parameters (the FWHM and centroid of the Gaussian and the $T_{1/2}$ value) are first left free to vary. To be considered as correct, the fit should give values of FWHM close to the one extrapolated from fig. 3 and a centroid value close to the expected one. If this is not the case, another fit is performed by constraining the Gaussian representing the prompt curve to have a FWHM and/or centroid value close to the expected ones. The measurement of the half-life of an excited state is obtained by analyzing several time spectra corresponding to delayed coincidences between the $\beta$-$BaF_2$, $\beta$-$LaBr_3$, and $BaF_2$-$LaBr_3$ detectors. Several fits of each time spectrum were performed by varying the number of spectrum channels used in order to test the influence of the background on the result. The dispersion observed on the results is taken into account to determine the error. The value we adopt for the half-life of the excited nuclear state studied is the mean (where each data is weighted inversely by its squared error) of the results obtained from the analysis of these various time spectra. If the half-life is found to be greater than or equal to 60 ps, the deconvolution method is applied. Otherwise, the centroid-shift method is used. In that case, the centroid of each time spectrum was calculated. The sensitivity of the result was studied as a function of the number of channels taken for the centroid determination and used to define the error on the centroid.

The analysis of the $T_{\beta\gamma}(\beta\text{-}463_{\mathrm{BaF_2}})$, $T_{\beta\gamma}(\beta\text{-}463_{\mathrm{LaBr_3}})$, $T_{\gamma\gamma}(409_{\mathrm{BaF_2}}\text{-}463_{\mathrm{LaBr_3}})$, $T_{\gamma\gamma}(463_{\mathrm{BaF_2}}\text{-}409_{\mathrm{LaBr_3}})$, $T_{\gamma\gamma}(547_{\mathrm{BaF_2}}\text{-}463_{\mathrm{LaBr_3}})$, and $T_{\gamma\gamma}(463_{\mathrm{BaF_2}}\text{-}547_{\mathrm{LaBr_3}})$ spectra has allowed us to determine the half-life of the 1899 keV level. Figure 5 shows three of these six time spectra. One can notice that the $T_{\beta\gamma}(\beta\text{-}463_{\mathrm{BaF_2}})$ and $T_{\beta\gamma}(\beta\text{-}463_{\mathrm{LaBr_3}})$ spectra do not yield the pure half-life of the 1899 keV level. Indeed, for these spectra, the $\beta$ branch is not uniquely defined, the half-lives of the levels located at higher energies and linked by $\gamma$-rays to the 1899 keV state can contribute to the measured slope. In the $^{138}$Ba level scheme, fourteen transitions feed the 1899 keV level; the sum of their total intensities represents 17.38% of the decay intensity, *i.e.* more than the direct feeding of the 1899 keV level

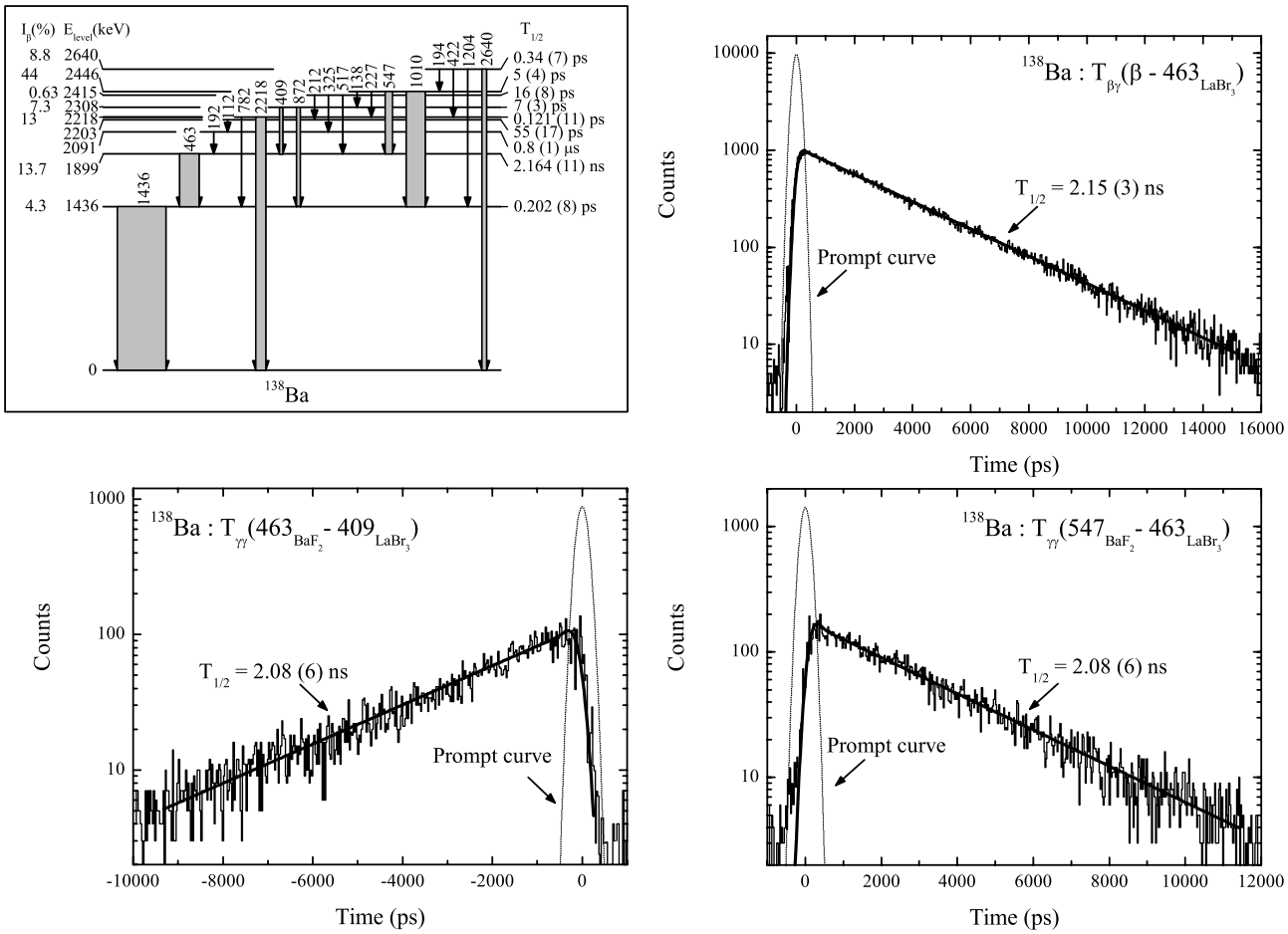


**Fig. 5.** Partial level scheme of $^{138}$Ba obtained from the decay of $^{138}$Cs; the arrow widths are proportional to the $\gamma$ intensity of the transitions; more than 90% of the decay intensity is displayed; data are taken from ref. [11]. Three time spectra for the half-life determination of the 1899 keV level of $^{138}$Ba; the solid line represents the best fit of the data, the half-life arising from the best fit is indicated.

(13.7%, see fig. 5). However, most of them have a very low intensity ($\leq$ 0.1%) and will not contribute significantly to the $T_{\beta\gamma}(\beta\text{-}463_{\mathrm{BaF_2}})$ and $T_{\beta\gamma}(\beta\text{-}463_{\mathrm{LaBr_3}})$ spectra. Only the four remaining transitions, namely the 192, 409, 517 and 547 keV transitions with total intensities equal to 0.60, 4.76, 0.43 and 10.87% respectively, could affect the $\beta$-$\gamma$ time spectra. The 409 and 547 keV transitions de-excite the 2308 and 2446 keV levels with very short half-lives (see fig. 5) that can be considered as negligible compared to the half-life of the 1899 keV level. The 192 keV transition de-excites the 2091 keV level that has a long half-life, 0.8 $\mu$s. But, taking into account the intensity of the 192 keV transition, we calculated that this third contribution will not change the $T_{1/2}$ value measured from the $\beta$-$\gamma$ time spectra by more than 0.1%, which is again negligible. The last contribution comes from the 2415 keV level with $T_{1/2}$ = 16 ps through the 517 keV transition. Here again, it is not significant because of the low intensity of the 517 keV transition. The $T_{1/2}$ values obtained from the analysis of the $\beta$-$\gamma$ time spectra, 2.14 (3) and 2.15 (3) ns, are fully compatible within error bars with those obtained from the analysis of the $\gamma$-$\gamma$ time spectra: 2.12 (6), 2.08 (6), 2.08 (6) and 2.06 (6) ns. Therefore, we adopted as the final result for the half-life of the 1899 keV level the mean of these six values: $T_{1/2}$ = 2.13 (3) ns, in excellent agreement with the value reported in the literature [11].

The total check of our measurement and analysis procedures would require the measurement of a half-life already known in the range of a few tens of ps. In the $^{138}$Ba level scheme, two excited nuclear states meet this requirement: the 2203 keV level with $T_{1/2}$ = 55 (17) ps and the 2415 keV level with $T_{1/2}$ = 16 (8) ps (see fig. 5). Both levels are very weakly fed by the $^{138}$Cs $\beta^-$ decay and the $\gamma$-rays involved in their de-excitation have very low intensities, more than ten times lower than the $\gamma$ lines for which we got results. Thus, unfortunately, we could not perform these measurements due to a lack of statistics.

### 3.2 A = 137 results

The $^{137}$Cs level scheme populated by the $^{137}$Xe $\beta^-$ decay is well known [13], but only an upper limit is reported for the half-life of the first excited state: $T_{1/2} \leq 0.1$ ns [14]. In

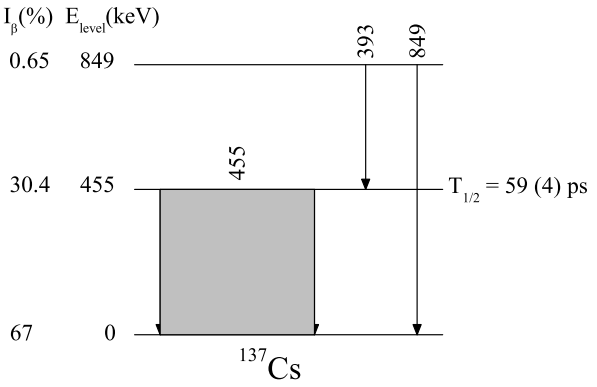


**Fig. 6.** Partial level scheme of $^{137}$Cs obtained from the decay of $^{137}$Xe; the arrow width is proportional to the $\gamma$ intensity of the transitions; data are taken from ref. [13], except the half-life (this work).

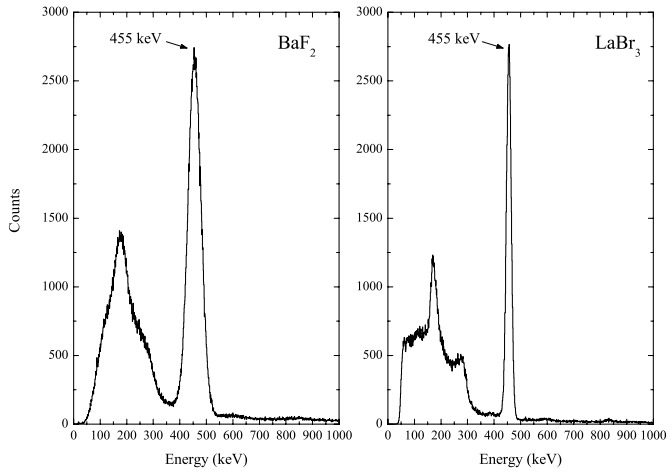


**Fig. 7.** $BaF_2$ and $LaBr_3$ projection spectra extracted from the $\mathcal{M}(E_\beta$-$E_{\mathrm{BaF_2}}$-$T_{\beta\text{-}\mathrm{BaF_2}})$ and $\mathcal{M}(E_\beta$-$E_{\mathrm{LaBr_3}}$-$T_{\beta\text{-}\mathrm{LaBr_3}})$ matrices by setting a gate defined by $\Delta E_{\beta min}$ and $\Delta E_{\beta max}$ (see sect. 2) on the $\beta$ detector.

$^{137}$Cs, the ground state and the first excited state located at 455.5 keV are fed, respectively, by 67 and 31% of the $^{137}$Xe $\beta^-$ decay (see fig. 6). The $\gamma$ spectrum exhibits almost exclusively the very strong 455.5 keV $\gamma$ line. Indeed, the absolute intensity of the 455.5 keV transition is equal to 31% against 0.6% for the second most intense $\gamma$ line (the 848.9 keV transition). Therefore, the half-life of the $^{137}$Cs first excited state can be measured by $\beta$-$\gamma$ delayed coincidences only: time spectra were extracted from the $\mathcal{M}(E_\beta$-$E_{\mathrm{BaF_2}}$-$T_{\beta\text{-}\mathrm{BaF_2}})$ and $\mathcal{M}(E_\beta$-$E_{\mathrm{LaBr_3}}$-$T_{\beta\text{-}\mathrm{LaBr_3}})$ matrices by selecting, in the $\beta$ detector, the gate defined by $\Delta E_{\beta min}$ and $\Delta E_{\beta max}$ (see sect. 2) and in the fast $\gamma$ detector the 455.5 keV $\gamma$ transition. The $\gamma$ spectra extracted from these matrices by using the same $\beta$ gate are displayed on fig. 7. The background under the 455 keV peaks appears to be very low. Thus it will not affect significantly the time spectra. We have verified this point by analyzing the time spectra obtained by setting gates on the full energy peak only, or subtracting also the contribution due

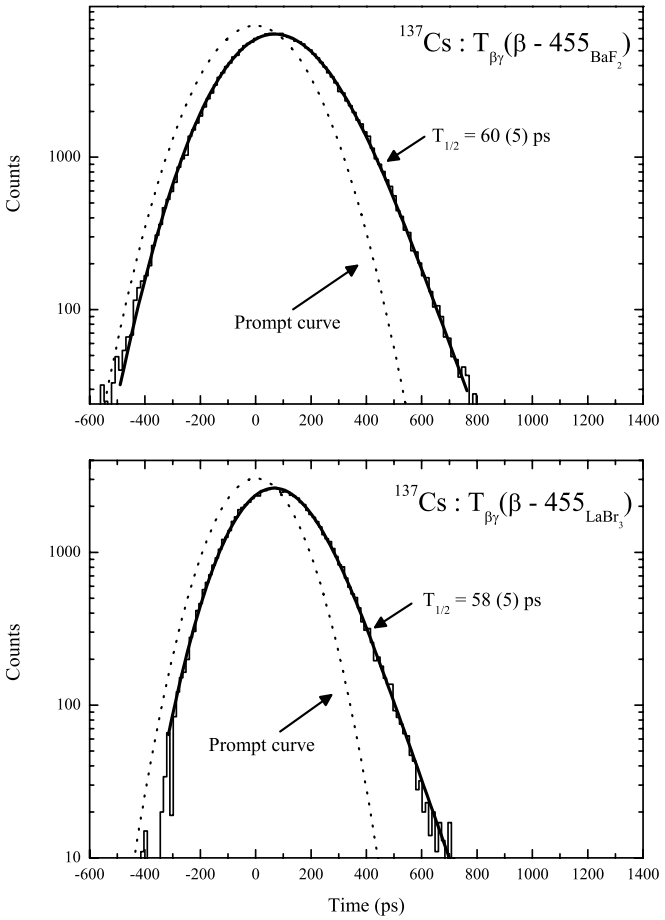


**Fig. 8.** Time spectra for the determination of the half-life of the 455.5 keV state in $^{137}$Cs; the solid line represents the best fit of the data, the half-life arising from the best fit is indicated.

the background located before and after the peak. The various time spectra exhibit only slight differences in the left tail of the peak and the intensity of these differences do not exceed some $10^{-3}$ of the peak maximum. Figure 8 shows typical time spectra obtained as well as the results of the deconvolution analysis. The analysis of all the time spectra has given consistent results: the widths of the Gaussians is found in excellent agreement with the values expected from the $A = 138$ results, and the dispersion observed on the $T_{1/2}$ results has been used to define the error bar. The value finally adopted for the half-life of the 455.5 keV level of $^{137}$Cs is: $T_{1/2}(455.5\,\mathrm{keV}) = 59\ (4)\,\mathrm{ps}$. And therefore the use of the deconvolution method is still justified.

### 3.3 A = 139 results

The $^{139}$Xe decay scheme to levels of $^{139}$Cs is well known [15], but up to now no half-life measurement has been reported for the $^{139}$Cs excited nuclear states. Figure 9 shows a partial low-lying level scheme of $^{139}$Cs as well as the half-life results obtained in this work. The half-life of the level located at 218 keV was determined from the analysis of four time spectra corresponding to $\gamma$-$\gamma$ delayed

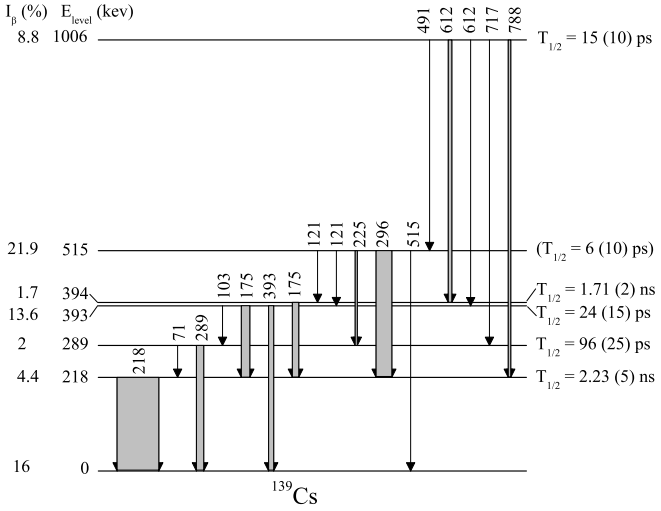


**Fig. 9.** Partial level scheme of $^{139}$Cs obtained from the decay of $^{139}$Xe; the arrow width is proportional to the $\gamma$ intensity of the transitions; data are taken from ref. [15], except the half-lives (this work).

coincidences. These four time spectra were obtained by selecting the 175-218 and 296-218 keV cascades (see fig. 9) on the energy axes of the $\mathcal{M}(E_{\mathrm{BaF_2}}\text{-}E_{\mathrm{LaBr_3}}\text{-}T_{\mathrm{BaF_2}\text{-}\mathrm{LaBr_3}})$ matrix. The time spectra corresponding to the 296-218 keV coincidence are not pure. Indeed two cascades involving $\gamma$-rays of very close energy, 225-289 keV and 296-218 keV, occur in the $^{139}$Cs level scheme (see fig. 9). With scintillators, despite the good energy resolution of $LaBr_3$, the 218-225 and 289-296 keV doublets cannot be separated (see fig. 2). Then the contributions arising from the 218 and 289 keV levels are mixed in the spectra labelled $T_{\gamma\gamma}(296_{\mathrm{BaF_2}}\text{-}218_{\mathrm{LaBr_3}})$ and $T_{\gamma\gamma}(218_{\mathrm{BaF_2}}\text{-}296_{\mathrm{LaBr_3}})$, and actually these spectra exhibit a very strong component due to a "long" half-life and a weak fast component. The comparison of the latter time spectra with the $T_{\gamma\gamma}(175_{\mathrm{BaF_2}}\text{-}218_{\mathrm{LaBr_3}})$ and $T_{\gamma\gamma}(218_{\mathrm{BaF_2}}\text{-}175_{\mathrm{LaBr_3}})$ ones shows that the "long" half-life has to be attributed to the 218 keV level. This attribution is corroborated by the relative $\gamma$ intensities of the 218, 225, 289, and 296 keV transitions (see fig. 9). The mean value obtained from the analysis of the four time spectra by the deconvolution method is: $T_{1/2}(218\,\mathrm{keV}) = 2.23\ (5)$ ns.

The 289 and 515 keV levels involve in their decay the 289, 225, and 296 keV transitions. As explained above, these $\gamma$ lines cannot be uniquely selected with the $BaF_2$ and $LaBr_3$ detectors. It was therefore necessary to use the $\beta$-$\gamma$-$\gamma$ triple-coincidence technique where the timing information is obtained from the $\beta$-$\gamma$ delayed coincidence between fast-timing detectors while the desired decay cascade is selected by a coincident $\gamma$-ray in the Ge(HP) detector.

Figure 10 shows the $LaBr_3$ coincidence spectra extracted from the $\mathcal{M}(E_{\mathrm{LaBr_3}}\text{-}E_{\mathrm{Ge}}\text{-}T_{\beta\text{-}\mathrm{LaBr_3}})$ matrix by gating the Ge(HP) detector on the 218 and 225 keV $\gamma$-rays. As expected from the level scheme (see fig. 9), the 289 keV $\gamma$-ray is observed in coincidence with the 225 keV transition and the 175 and 296 keV lines with the 218 keV transition. We can note that the 289 and 296 keV peaks are superimposed on an almost zero background that will not affect the corresponding time spectra.

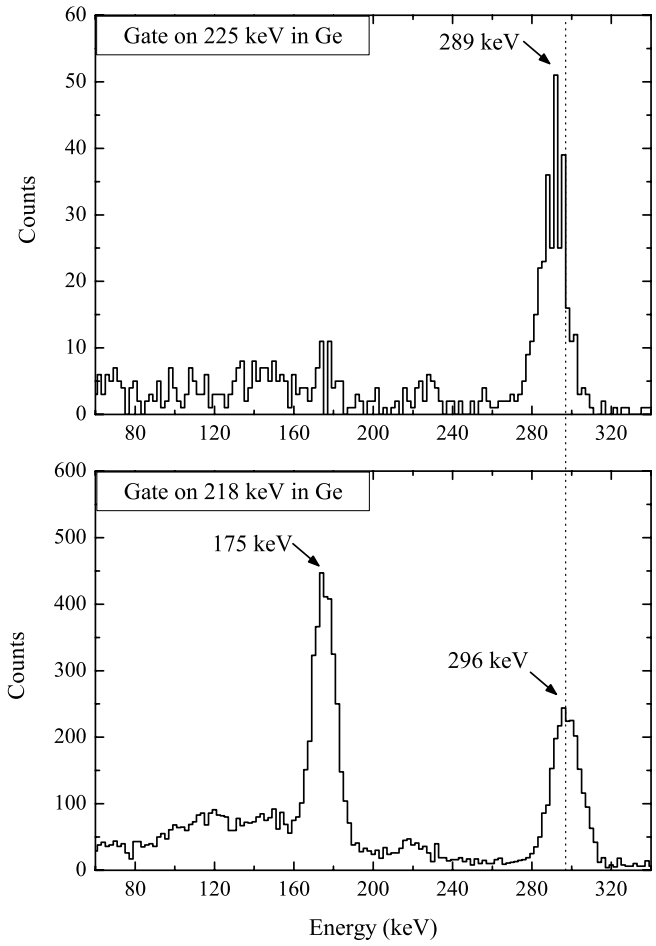


**Fig. 10.** $LaBr_3$ projection spectra extracted from the $\mathcal{M}(E_{\mathrm{LaBr_3}}\text{-}E_{\mathrm{Ge}}\text{-}T_{\beta\text{-}\mathrm{LaBr_3}})$ matrix by gating the Ge(HP) detector on the 218 and 225 keV $\gamma$-rays.

By setting on the Ge(HP) detector a gate on the 225 keV $\gamma$ line and on the fast detector a gate on the 289 keV $\gamma$-ray, the $\beta$-225-289 keV cascade is selected (see fig. 9). Such time spectra have been extracted from the $\mathcal{M}(E_{\mathrm{X}}\text{-}E_{\mathrm{Ge}}\text{-}T_{\beta\text{-}\mathrm{X}})$ matrices (X standing for $BaF_2$ or $LaBr_3$). The sum of the half-lives of the 515 and 289 keV levels can be obtained from the analysis of these time spectra, if we neglect the effect induced by the transitions feeding the level at 515 keV (this point will be discussed in the next paragraph). These multi-gated spectra have low statistics (see as an example the $T_{\beta\gamma}(\beta\text{-}289_{\mathrm{LaBr_3}}\text{-}225_{\mathrm{Ge}})$ spectrum in fig. 11), but they exhibit clearly a slope. And so by fitting these time spectra by the function resulting from the convolution of a Gaussian function and an exponential function, we can determine, with a large error bar, the sum of the half-lives of the 515 and 289 keV levels: $T_{1/2}(515\,\mathrm{keV}) + T_{1/2}(289\,\mathrm{keV}) = 105\ (30)$ ps. For such a value, the analysis by the deconvolution method is fully justified. To check our ability to determine half-lives by

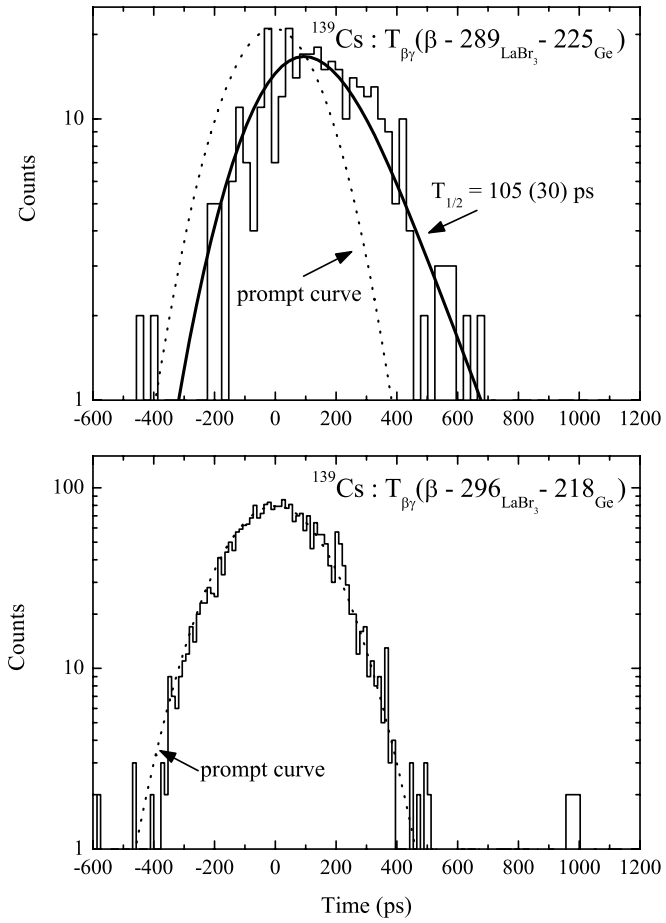


**Fig. 11.** Time spectra for the half-life determination of levels in $^{139}$Cs. The upper spectrum gives access to $T_{1/2}(515\,\mathrm{keV}) + T_{1/2}(289\,\mathrm{keV})$, the lower spectrum to $T_{1/2}(515\,\mathrm{keV})$.

the centroid-shift method, we have analyzed, using this method, the $T_{\beta\gamma}$ ($\beta$-289$_{\mathrm{LaBr_3}}$-225$_{\mathrm{Ge}}$) and $T_{\beta\gamma}$ ($\beta$-289$_{\mathrm{BaF_2}}$-225$_{\mathrm{Ge}}$) spectra. The mean of the results obtained is $T_{1/2}$ (515 keV) + $T_{1/2}$(289 keV) = 102 (15) ps, the error taking into account the accuracy on the centroid expected for the prompt curve and the sensitivity of the result to the number of spectrum channels used in the centroid determination (in other word, the sensitivity to the background). The results obtained by both methods are in quite good agreement.

In the $^{139}$Cs level scheme, the 218 keV transition is in coincidence not only with the 296 keV $\gamma$-ray but also with the 175 keV $\gamma$ lines (see figs. 9 and 10). Therefore, in order to select uniquely the $\beta$-296-218 keV decay path and measure the half-life of the 515 keV level, it is necessary to define two energy gates: the first one, on the Ge(HP) detector, set on the 218 keV $\gamma$ line and the second one, on the fast detector, set on the 296 keV $\gamma$-ray; such time spectra were extracted from the $\mathcal{M}(E_{\mathrm{BaF_2}}$-$E_{\mathrm{Ge}}$-$T_{\beta\text{-}\mathrm{BaF_2}})$ and $\mathcal{M}(E_{\mathrm{LaBr_3}}$-$E_{\mathrm{Ge}}$-$T_{\beta\text{-}\mathrm{LaBr_3}})$ matrices. Strictly speaking these spectra will contain contributions due to the half-lives of the states located at higher energies and connected by transitions to the 515 keV level. But, in the present case, these contributions can be neglected. The feeding of the 515 keV level by $\gamma$ transitions represents 4.94% of the total decay intensity, so it is well below the direct feeding of this level (see fig. 9). Most of the eighteen transitions feeding the 515 keV level have a very low intensity ($\leq$ 0.36%), except for two transitions: the 491 keV one, with a 1.4% intensity, which depopulates the 1006 keV level (see fig. 9) and a 1670 keV transition, with a 1.1% intensity, that depopulates a 2185 keV level not reported in fig. 9. We calculated that the half-lives of the 1006 and 2185 keV levels should be more than a few hundred picoseconds to have a detectable effect on the considered time spectra, which is not the case for the 1006 keV level (see fig. 9) and highly unlikely for the 2185 keV state that decays mostly by high-energy ($\sim$ 1500 keV) $\gamma$-rays. The $T_{\beta\gamma}$($\beta$-296$_{\mathrm{LaBr_3}}$-218$_{\mathrm{Ge}}$) time spectrum, shown in fig. 11, does not exhibit a significant slope. The analysis of this experimental spectrum by the deconvolution method leads to $T_{1/2} = 7^{+15}_{-7}$ ps for the half-life of the 515 keV level. This value is below the lower limit adopted for a reliable use of the deconvolution method (see sect. 3.1). Therefore we analyzed the $T_{\beta\gamma}$($\beta$-296$_{\mathrm{LaBr_3}}$-218$_{\mathrm{Ge}}$) and $T_{\beta\gamma}$($\beta$-296$_{\mathrm{BaF_2}}$-218$_{\mathrm{Ge}}$) time spectra using the centroid-shift method, and obtained $T_{1/2}$ = 6 (10) ps for the half-life of the 515 keV level. This very short value can be below the limit that can be expected in our experiment using the centroid-shift method and must be considered only as a rough measurement of the half-life of the 515 keV level. Using this estimate, the half-life of the level located at 289 keV is deduced to be: $T_{1/2}$(289 keV) = 96 (25) ps. It is worth noting that, in order to measure the sum of the half-lives of the levels located at 289 and 515 keV on the one hand and the half-life of the 515 keV level on the other hand, the signals used as stop for the TAC have very similar energies, 289 and 296 keV, respectively. In this case, the centroids of the corresponding prompt curves differ by around 3 ps. Neglecting this small difference, we can measure the half-life of the 289 keV level directly from the centroid shift between the $T_{\beta\gamma}$($\beta$-289$_{\mathrm{LaBr_3}}$-225$_{\mathrm{Ge}}$) and $T_{\beta\gamma}$($\beta$-296$_{\mathrm{LaBr_3}}$-218$_{\mathrm{Ge}}$) time spectra or between the $T_{\beta\gamma}$($\beta$-289$_{\mathrm{BaF_2}}$-225$_{\mathrm{Ge}}$) and $T_{\beta\gamma}$($\beta$-296$_{\mathrm{BaF_2}}$-218$_{\mathrm{Ge}}$) ones, which leads to $T_{1/2}$(289 keV) = 99 (15) ps, a value quite consistent with that reported above from the centroid shift between the prompt curves and the experimental spectra. The result found for the half-life of the 289 keV level does not depend on the absolute positions of the prompt curves at 289 and 296 keV, but only on the difference between their positions; thus the determined value, $T_{1/2}$(289 keV) = 96 (25) ps, is quite accurate.

The $^{139}$Cs level scheme exhibits a close-lying doublet at 393 and 394 keV [15], both levels decaying by a 175 keV transition. Ten excited states of higher energies de-excite to them, in particular the previously discussed 1006 keV level that is connected to the doublet via 612 keV transitions (see fig. 9). However the 393 keV level decays also via a second strong transition, the 393 keV one. Therefore, the time spectra corresponding to delayed coincidences involving the 175 keV $\gamma$ line will show two contributions due to the half-lives of the 393 and 394 keV levels whereas

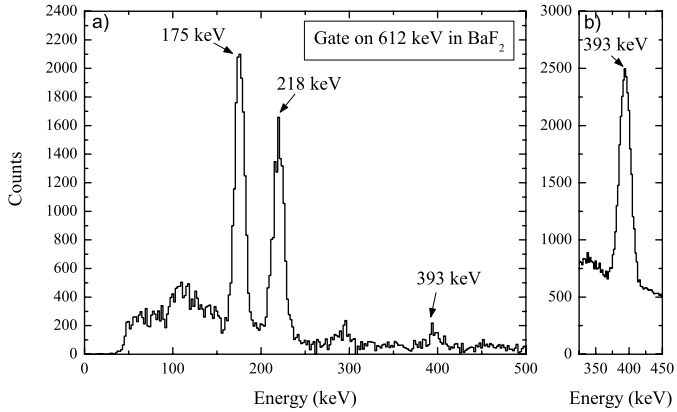


**Fig. 12.** a) $LaBr_3$ projection spectrum extracted from the $\mathcal{M}(E_{BaF_2}$-$E_{LaBr_3}$-$T_{BaF_2\text{-}LaBr_3})$ matrix by gating the $BaF_2$ detector on the 612 keV $\gamma$ line. b) Partial $LaBr_3$ projection spectrum extracted from the $\mathcal{M}(E_\beta$-$E_{LaBr_3}$-$T_{\beta\text{-}LaBr_3})$ matrix by setting on the $\beta$ detector the gate defined by $\Delta E_{\beta min}$ and $\Delta E_{\beta max}$.

the time spectra involving the 393 keV line will exhibit only one contribution due to the half-life of the 393 keV level. Figure 12a) shows the $LaBr_3$ coincidence spectrum extracted from the $\mathcal{M}(E_{BaF_2}$-$E_{LaBr_3}$-$T_{BaF_2\text{-}LaBr_3})$ matrix by gating the $BaF_2$ detector on the 612 keV $\gamma$-ray. The 175 and 218 keV $\gamma$ lines appear clearly on the spectrum which exhibits a rather low background. In order to check the influence of this background on the results, in addition to the time spectra obtained by selecting the 612-175 keV cascade in the fast detectors, we extracted from the $\mathcal{M}(E_{BaF_2}$-$E_{LaBr_3}$-$T_{BaF_2\text{-}LaBr_3})$ matrix the time spectrum corresponding to gates set on 612 keV in the $BaF_2$ detector and on the background above the 175 keV $\gamma$ line in the $LaBr_3$ detector. In this spectrum a small tail appears on the right side of the peak, it is due to the Compton from the 218 keV transition that de-excites the long-lived ($T_{1/2}$ = 2.23 ns) level located at 218 keV. Such a Compton contribution was eliminated by subtracting this time spectrum obtained by gating on the Compton continuum from the one obtained by gating on the full-energy 175 keV peak. The analysis of the time spectra obtained with or without subtraction of the Compton background leads to the same $T_{1/2}$ value, which shows that the Compton background below the 175 keV peak does not affect the half-life determination and then cannot be responsible for the "long" half-life observed in fig. 13. In order to determine whether the 1.7 ns half-life has to be associated with the level located at 393 keV or to the one at 394 keV, the time spectra corresponding to the delayed coincidences involving the 393 keV transition were analyzed. In fig. 12a), the 393 keV $\gamma$ line appears as a very weak peak. Therefore time spectra extracted from the $\mathcal{M}(E_{BaF_2}$-$E_{LaBr_3}$-$T_{BaF_2\text{-}LaBr_3})$ matrix by selecting the 612-393 keV cascade in the fast detectors are not relevant. By setting on the $\beta$ detector the $\Delta E_{min}$-$\Delta E_{max}$ gate (see sect. 2), we obtained from another matrix, the $\mathcal{M}(\beta$-$E_{LaBr_3}$-$T_{\beta\text{-}LaBr_3})$ one, the coincident $\gamma$-energy spectrum partially displayed in fig. 12b). In this latter spectrum, the 393 keV $\gamma$ line is strong but

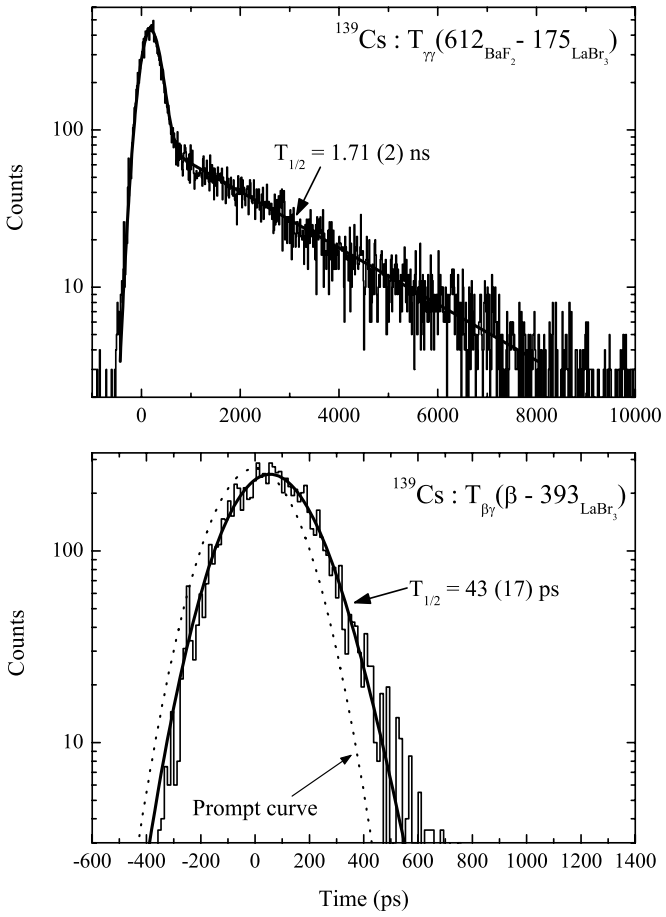


**Fig. 13.** Time spectra for the half-life determination of excited levels in $^{139}$Cs. The upper spectrum shows two components due to the half-lives of the 393 and 394 keV levels, the lower spectrum gives access to $T_{1/2}$(393 keV).

it is superimposed to a rather large background. However, the time spectrum extracted from this matrix and corresponding to a gate set on the background above the 393 keV line shows that the Compton background contains no long-lived component. The analysis of the time spectra, extracted from the $\mathcal{M}(\beta$-$E_{LaBr_3}$-$T_{\beta\text{-}LaBr_3})$ and $\mathcal{M}(\beta$-$E_{BaF_2}$-$T_{\beta\text{-}BaF_2})$ matrices, for the 393 keV transition with subtraction of the Compton background was performed at first by the deconvolution method but the result obtained, $T_{1/2}$ = 43 (17) ps, shown in fig. 13, is lower than the limit adopted in sect. 3.1 for a reliable use of the deconvolution method. Then the time spectra were analyzed with the centroid-shift method, the result obtained, $T_{1/2}$ = 24 (15) ps, is slightly lower (but consistent within the errors bars) than the value found by the deconvolution method. A contribution of higher-energy levels to the half-life measured with these $\beta$-$\gamma$ delayed-coincidence time spectra could occur. Indeed the level located at 393 keV is fed by many transitions (some of them belong to doublets with partners which feed also the 394 keV state), but most of these transitions have a very low intensity and cannot affect the result obtained. As an example, the most intense one, the 612 keV transition, represents less

than 10% of the direct feeding of the 393 keV level, thus the contribution of the half-life of the 1006 keV level can be neglected. Therefore we adopt the following half-life for the 393 keV level: $T_{1/2}(393\,\mathrm{keV}) = 24\ (15)$ ps. In any case, we have demonstrated that the half-life of the level that decays by the 393 keV transition is short and therefore we can attribute the "long" half-life value to the 394 keV level: $T_{1/2}(394\,\mathrm{keV}) = 1.71\ (2)$ ns.

The time spectra extracted from the $\mathcal{M}(E_\beta\text{-}E_{\mathrm{BaF_2}}\text{-}T_{\beta\text{-}\mathrm{BaF_2}})$ and $\mathcal{M}(E_\beta\text{-}E_{\mathrm{LaBr_3}}\text{-}T_{\beta\text{-}\mathrm{LaBr_3}})$ matrices by selecting in the fast $\gamma$ detector the 612 or 788 keV $\gamma$ transitions have allowed us to determine the half-life of the level located at 1006 keV. The analysis by the deconvolution method leads to a half-life lower than 60 ps, thus we applied the centroid-shift method and obtained: $T_{1/2}$ (1006 keV) = 15 (10) ps. Here again we have assumed that the contributions of the higher-energy states linked by $\gamma$-rays to the 1006 keV level can be neglected, which seems justified since the seven transitions feeding the 1006 keV level represent 1.64% of the total decay intensity while the direct feeding of the 1006 keV level is equal to 8.8%.

Finally, from the half-lives measured in this work, we calculated the $M1$ and $E2$ reduced transition probabilities for the transitions de-exciting the first excited levels in $^{137,139}$Cs. These values are reported in table 1.

## 4 Discussion

The $^{137}$Cs nucleus has $\frac{7}{2}^+$ and $\frac{5}{2}^+$ as spin and parity values for its ground and first excited states, respectively [13]. Such $\frac{7}{2}^+$ and $\frac{5}{2}^+$ states are present at low energy in all the $N = 82$ isotones from $^{133}$Sb to $^{145}$Eu and the results from stripping and pickup reactions have shown that these states correspond to $\pi 1g_{7/2}$ and $\pi 2d_{5/2}$ configurations [17]. Moreover, with the exception of the $^{136}$Xe(d, $^3$He) $^{135}$I reaction where two $l_p = 2$ transitions corresponding to the pickup of a $2d_{5/2}$ proton were observed, the single-particle (hole) strengths for the $\pi 1g_{7/2}$ and $\pi 2d_{5/2}$ orbitals are concentrated into single levels. The transition linking the $\frac{5}{2}^+$ and $\frac{7}{2}^+$ states in the $N = 82$ isotones is then the $\pi 2d_{5/2} \rightarrow \pi 1g_{7/2}$ $l$-forbidden $M1$ transition.

In $^{139}$Cs, the spin and parity values have been determined without ambiguity only for the ground state: $\mathrm{I}^\pi = \frac{7}{2}^+$ [15]. The levels at 218.6, 289.8, 393.5, and 393.8 keV are given in ref. [15] as $\frac{5}{2}$ or $\frac{7}{2}^+$, $\frac{3}{2}$ or $\frac{5}{2}$ or $\frac{7}{2}^+$, $\frac{5}{2}(^+)$ or $\frac{7}{2}^+$, and $\frac{3}{2}$ or $\frac{5}{2}$ or $\frac{7}{2}^+$, respectively. However, from systematic behaviour through the Cs isotopes [18] and angular correlation measurement results [19], $\mathrm{I}^\pi = \frac{5}{2}^+$ seems to be the most probable spin and parity value for the first excited level located at 218.6 keV. The $\frac{7}{2}^+$ and $\frac{5}{2}{}^+_1$ in the $N = 84$ isotones have also been interpreted as originating from the $\pi 1g_{7/2}$ and $\pi 2d_{5/2}$ orbitals. Thus the $\frac{5}{2}{}^+_1 \rightarrow \frac{7}{2}^+$ transition in $^{139}$Cs could be the $\pi 2d_{5/2} \rightarrow \pi 1g_{7/2}$ $l$-forbidden $M1$ transition.

Figure 14 shows the $M1$ hindrance factors relative to the Weisskopf estimate for the $\frac{5}{2}{}^+_1 \rightarrow \frac{7}{2}^+$ transitions known in the Sb ($Z = 51$) to Eu ($Z = 63$) isotopes. The $F_W(M1)$ behaviour is very similar through the $N = 82$ and 84 isotones; in both cases, $F_W(M1)$ decreases rather regularly when the proton number increases. In the Sb ($Z = 51$) and I ($Z = 53$) isotope series, the $F_W(M1)$ values are all the higher as the neutron number comes closer to the $N = 82$ magic number. In the Cs ($Z = 55$), La ($Z = 57$) and Pr ($Z = 59$) isotopes, the change in the $F_W(M1)$ values as a function of the neutron number is less regular. However, in these nuclei, except for $N = 82$, two $\frac{5}{2}^+$ states lie at low energy; one corresponds mainly to the one-proton state issued from the $\pi 2d_{5/2}$ orbital and the other one either to the $\left(1g\frac{7}{2}\right)^{-3}_{\frac{5}{2}}$ three-hole state or to the $\frac{5}{2}^+$ member of the $2^+_1 \otimes \frac{7}{2}^+$ multiplet originating from the coupling of the $2^+_1$ state of the core with the $\frac{7}{2}^+$ single quasi-particle state. And it is worth noting that, when both the $M1$ hindrance factors corresponding to the $\frac{5}{2}{}^+_1 \rightarrow \frac{7}{2}^+$ and $\frac{5}{2}{}^+_2 \rightarrow \frac{7}{2}^+$ transitions are known, the higher value is sometimes found for the $\frac{5}{2}{}^+_2$ state, as in $^{133}$Cs and $^{133}$La [27]. Moreover, in calculations performed in the frame of the intermediate-coupling unified nuclear model for $^{133}$Cs [36], the $\frac{5}{2}{}^+_2$ state has been interpreted as arising from the coupling of the single odd proton in the $2d_{5/2}$ orbital to the $^{132}$Xe core. Finally it appears clearly in fig. 14 that the closer to the $Z = 50$, $N = 82$ closed shells the nucleus is, the more appropriate the description in terms of single-particle states is, the larger the contribution of the $2d_{5/2}$ orbital to the $\frac{5}{2}{}^+_1$ state is, and then the higher the $F_W\left(M1; \frac{5}{2}{}^+_1 \rightarrow \frac{7}{2}^+\right)$ value is. This statement is fully supported by the $M1$ hindrance factors obtained for the 455.5 and 218.6 keV transitions in $^{137}$Cs$_{82}$ and $^{139}$Cs$_{84}$, respectively.

It follows from the foregoing that the first excited state in $^{139}$Cs is undoubtedly the $\frac{5}{2}^+$ state corresponding to the $\pi 2d_{5/2}$ configuration. Let us now consider the states located at higher energy. The similarity between the properties of the low-lying states in $^{133}$Cs, $^{139}$Cs and $^{141}$La has already been emphasized in ref. [19]. The $2^+$ states in the respective cores lie at approximately the same energy: 667.7 keV in $^{132}$Xe with four neutron holes in the $N = 82$ closed shell and 588.8 and 602.3 keV in $^{138}$Xe and $^{140}$Ba with two neutrons beyond the closed shell. And in the odd-A nuclei $^{133}$Cs and $^{141}$La, the first excited states are a pair of $\frac{5}{2}^+$ levels and then two states with spin and parity values $\frac{3}{2}^+$ and $\frac{1}{2}^+$. One can see, in fig. 15, that in $^{139}$Cs the first four excited states exhibit decay modes quite similar to those observed in $^{141}$La. A one-by-one level identification is straightforward for the first three excited states and leads us to propose the spin and parity values $\frac{5}{2}^+$ and $\frac{3}{2}^+$ for the 289.8 and 393.5 keV levels, respectively. In this case, the 393.5 keV transition has to be an $E2$ transition, which is consistent with the conversion coefficient measurements [16] that yield $E2$ as the most probable multipolarity. Therefore, the 393.8 keV level could have $\frac{1}{2}^+$

**Table 1.** $M1$ and $E2$ reduced transition probabilities, in Weisskopf units, for the transitions de-exciting the first excited levels in $^{137,139}$Cs. The multipolarity of the transitions is taken from ref. [16]. The 175.0 keV transition, not known as a doublet in ref. [16], was reported as a $M1(E2)$ transition; here, one of the 175.0 keV transitions is assumed to have the $E2$ multipolarity and the other one the $M1$ multipolarity.

| Nucleus | $E_{level}$ (keV) | $T_{1/2}$ | $E_\gamma$ (keV) | Multipolarity | $B(M1)$ | $B(E2)$ |
|---|---|---|---|---|---|---|
| $^{137}$Cs | 455.5 | 59(4) ps | 455.5 | $E2$ ($\leq 10\%$ $M1$) | $\leq 0.00041$ | 11.0(13) |
| $^{139}$Cs | 218.6 | 2.23(5) ns | 218.6 | $M1 + E2$ ($41 \pm 2\%$) | 0.00035(3) | 6.3(4) |
| $^{139}$Cs | 289.8 | 96(25) ps | 71.0 | $M1$, $E2$ | $\leq 0.012$ | $\leq 1384$ |
| | | | 289.8 | $M1$, $E2$ | $\leq 0.0083$ | $\leq 59$ |
| $^{139}$Cs | 393.5 | 24(15) ps | 103.7 | $M1$ ($\leq 45\%E2$) | 0.011(7) | $< 818$ |
| | | | 175.0 | $M1$ | $0.09^{+0.15}_{-0.04}$ | |
| | | | 393.5 | $E2$ ($\leq 70\%$ $M1$) | $\leq 0.009$ | 26(23) |
| $^{139}$Cs | 393.8 | 1.71(2) ns | 175.0 | $E2$ | | 37(1) |

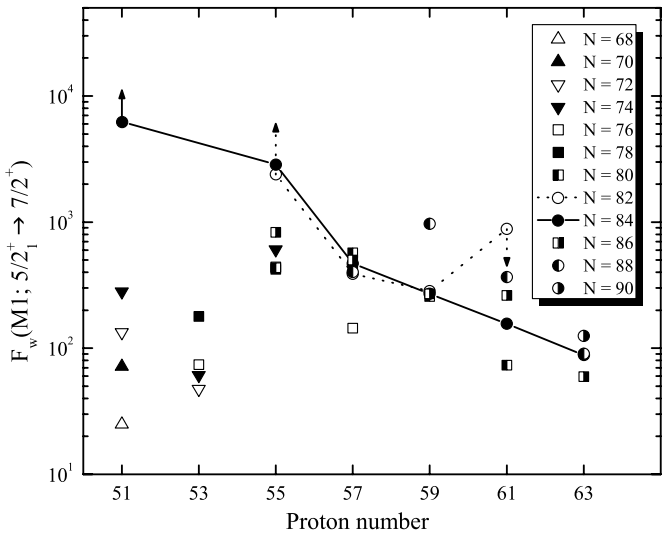


**Fig. 14.** Weisskopf $M1$ hindrance factors for the $\frac{5}{2}{}^+_1 \rightarrow \frac{7}{2}{}^+$ transitions known in the Sb to Eu isotopes. Data are taken from refs. [13,15,20–35]. When the $\frac{5}{2}{}^+_1$ state is the ground state, the experimental $B(M1)$ used to calculate the hindrance factor was modified by the $\frac{8}{6}$ factor corresponding to $(2I_i + 1)/(2I_f + 1)$.

as spin and parity value. This suggestion already made in ref. [19] was dismissed by the evaluator for lack of consistency with the probable dipole nature of the 175.0 keV transition [15]. This argument is rather weak. Indeed, it is worth reminding that, when the $^{139}$Cs transition multipolarities were measured, the existence of the 175.0 keV $\gamma$-ray doublet had not yet been demonstrated. Moreover, in Cs the conversion coefficients for the $M1$ or $E2$ multipolarity differ from one another by less than 20%; besides, in ref. [16] the $E2$ multipolarity was not ruled out for the 175.0 keV transition. In the following, we assume, for that matter, the $E2$ multipolarity for the 175.0 keV transition de-exciting the 393.8 keV level. Table 2 presents the reduced transition probabilities for the transitions de-exciting the first four excited levels in $^{133}$Cs and $^{139}$Cs. The $^{141}$La nucleus is not listed in this table, only the half-life of its 190.3 keV level being measured. The $B(M1)$ value calculated in ref. [29] for the 190.3 keV transition, 0.00213 (11) W.u., is similar to that obtained for the 81.0 keV transition in $^{133}$Cs, which is expected considering the equal distance in number of nucleons, 9, from the closed shells: five protons and four neutron holes for $^{133}$Cs and seven protons and two neutrons for $^{141}$La. The difference between the $B(M1)$ values for the transitions de-exciting the second excited state in $^{133}$Cs and $^{139}$Cs (see table 2) probably results, as indicated above for the first excited state, from changes in the nature and purity of the two $\frac{5}{2}{}^+$ states with the distance to the $N = 82$ magic shell (4 neutron holes compared to 2 neutrons). The reduced transition probabilities for the transitions de-exciting the 383.8 and 393.5 keV levels in $^{133}$Cs and $^{139}$Cs (see table 2) are rather similar, which strengthens the $\frac{3}{2}{}^+$ assignment to the spin and parity value of the 393.5 keV level in $^{139}$Cs. With regard to the fourth excited state, in $^{139}$Cs it decays only to the $\frac{5}{2}{}^+_1$ level. In $^{133}$Cs and $^{141}$La (see fig. 15), another strong-decay path leads to the $\frac{3}{2}{}^+$ state. The corresponding transition cannot exist in $^{139}$Cs because of the quasi-degeneracy of the 393.5 and 393.8 keV levels. In $^{133}$Cs only a lower limit is known for the $B(E2)$ value of the $\frac{1}{2}{}^+ \rightarrow \frac{5}{2}{}^+_1$ transition. However this transition has been observed in $^{121}$Sb and $^{121,123,125,127}$I and the corresponding reduced $E2$ transition probabilities are equal to 25, 78, 63, 34 and 24 W.u. [21–24]. The $B(E2)$ value obtained for the 175.0 keV transition in $^{139}$Cs fits in well with this set. So we propose to consider the 393.8 keV level as the $\frac{1}{2}{}^+$ state in $^{139}$Cs.

The spin values suggested above for the excited states of $^{139}$Cs could be supported by half-life measurements for the excited states of $^{141}$La, isotone of $^{139}$Cs. Moreover, it

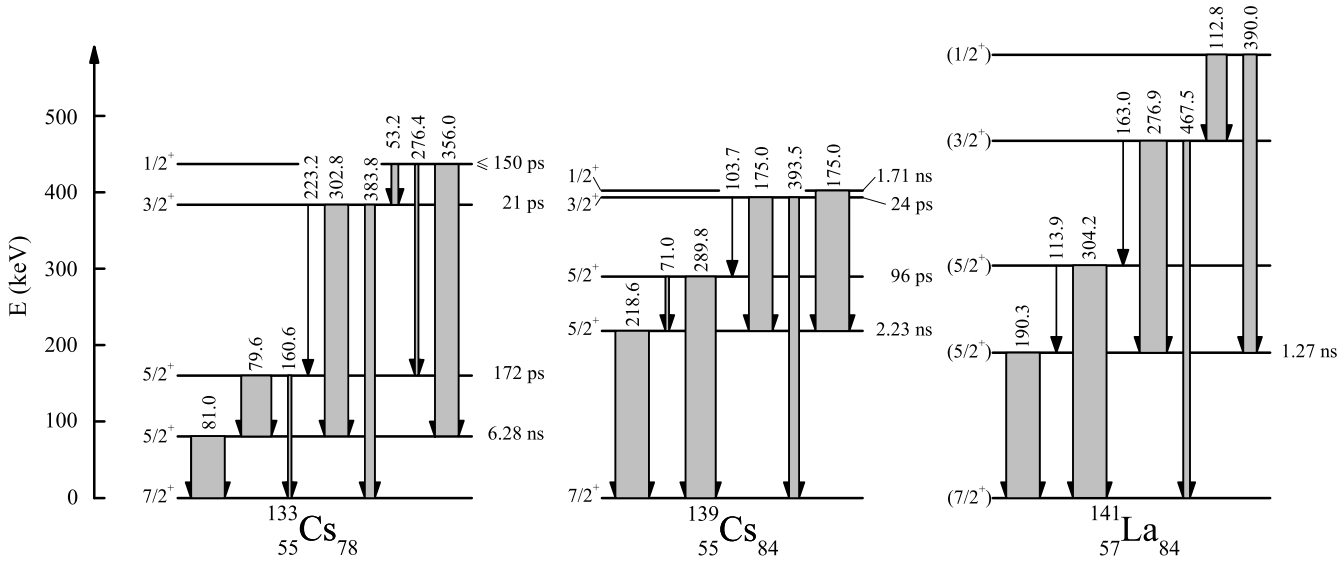


**Fig. 15.** Comparison between the first four excited levels in $^{133,139}$Cs and $^{141}$La. The experimental data were taken from this work and refs. [15,27,29]. The transition energies are indicated in keV. The arrow width is proportional to the total intensity of the transitions. For each level, the sum of the total intensities of the transitions has been normalized to 100.

**Table 2.** Reduced transition probabilities, in Weisskopf units, for the transitions de-exciting the first excited levels in $^{133,139}$Cs. The initial-level and transition energies are indicated in keV in the first and second columns of each block; the spin and parity values of the levels linked by the transition are indicated in the third column of each block.

| $^{133}$Cs [27] | | | | | $^{139}$Cs (this work) | | | | |
|---|---|---|---|---|---|---|---|---|---|
| $E_i$ | $E_\gamma$ | $I_i^\pi \rightarrow I_f^\pi$ | $B(M1)$ | $B(E2)$ | $E_i$ | $E_\gamma$ | $I_i^\pi \rightarrow I_f^\pi$ | $B(M1)$ | $B(E2)$ |
| 81.0 | 81.0 | $5/2^+ \rightarrow 7/2^+$ | 0.00237(5) | 5.25(17) | 218.6 | 218.6 | $5/2^+ \rightarrow 7/2^+$ | 0.00035(3) | 6.3(4) |
| 160.6 | 79.6 | $5/2^+ \rightarrow 5/2^+$ | 0.077(8) | 120(30) | 289.8 | 71.0 | $5/2^+ \rightarrow 5/2^+$ | $\leq 0.012$ | $\leq 1384$ |
| | 160.6 | $5/2^+ \rightarrow 7/2^+$ | 0.00117 (12) | 27(3) | | 289.8 | $5/2^+ \rightarrow 7/2^+$ | $\leq 0.0083$ | $\leq 59$ |
| 383.8 | 223.2 | $3/2^+ \rightarrow 5/2^+$ | 0.00145(22) | 0.24(7) | 393.5 | 103.7 | $3/2^+ \rightarrow 5/2^+$ | 0.011(7) | $< 818$ |
| | 302.8 | $3/2^+ \rightarrow 5/2^+$ | 0.024(4) | $< 190$ | | 175.0 | $3/2^+ \rightarrow 5/2^+$ | $0.09^{+0.15}_{-0.04}$ | |
| | 383.8 | $3/2^+ \rightarrow 7/2^+$ | | 25 | | 393.5 | $3/2^+ \rightarrow 7/2^+$ | $\leq 0.009$ | 26(23) |
| 437.0 | 53.2 | $1/2^+ \rightarrow 3/2^+$ | $> 0.023$ | $> 25$ | 393.8 | | | | |
| | 276.4 | $1/2^+ \rightarrow 5/2^+$ | | $> 4.8$ | | | | | |
| | 356.0 | $1/2^+ \rightarrow 5/2^+$ | | $> 12$ | | 175.0 | $1/2^+ \rightarrow 5/2^+$ | | 37(1) |

would be interesting to compare the $^{137,139}$Cs experimental transition probabilities to results of shell-model calculations. Indeed such a comparison would be a good test of the shell-model interactions close to $N = 82$. Shell-model calculations have been reported for the high-spin states of $^{139}$Cs by Liu *et al.* [37]: the 218 keV state was assigned to have a spin $\frac{5}{2}^+$, its energy is rather well reproduced by the calculations but no theoretical transition probabilities are reported for $^{139}$Cs.

## 5 Conclusions

A fast-timing setup has been developed to measure the half-life of excited states in neutron-rich nuclei. The first on-line experiment has been achieved successfully on the $^{137,139}$Cs levels populated by the $\beta^-$ decay of the $^{137,139}$Xe nuclei produced with the ALTO facility. In $^{137}$Cs, the half-life of the first excited state was measured to be $T_{1/2} = 59\ (4)$ ps. For the half-life determination in $^{139}$Cs, it was essential to use the $\beta$-$\gamma$-$\gamma$ technique where the $\beta$-$\gamma$ delayed coincidence spectra are obtained with an additional energy condition set on the Ge(HP) detector in order to select specifically the decay path. In this way, we could determine the half-lives of the levels located at 218.6, 289.8, 393.5 and 393.8 keV in $^{139}$Cs: $T_{1/2} = 2.23\ (5)$ ns, 96 (25) ps, 24 (15) ps and 1.71 (2) ns, respectively. In $^{137,139}$Cs, the high value found for the hindrance factor of the $\frac{5}{2}^+_1 \rightarrow \frac{7}{2}^+$ transition confirms that the first excited $\frac{5}{2}^+$ state corresponds mainly to the one-proton state issued from the $\pi 2d_{5/2}$ orbital. The $B(M1)$ and $B(E2)$ analysis for the transitions de-exciting the first excited levels in $^{139}$Cs as well as the comparison with the neighboring nuclei, in particular $^{133}$Cs and $^{141}$La, lead us to suggest the spin and parity assignments $\frac{5}{2}^+$, $\frac{3}{2}^+$, and $\frac{1}{2}^+$ for the levels located at 289.8, 393.5, and 393.8 keV.

We would like to thank the ALTO staff for their technical assistance and cooperation before and during the experiment. We thank also K. Nguyen-Kim for his technical help in the setting-up of the data acquisition system. One of us (BR) is grateful to Dr. J. Sauvage for her continuous interest in this work and stimulating discussions. Two of us (MAC and DH) would like to thank the Institut de Physique Nucléaire d'Orsay for the financial support granted during their stays in Orsay. The French Bulgarian Collaboration is grateful to the French Ministère des Affaires Etrangères et Européennes for the financial support granted via the ECONET program (project 21331RH).

## References

1. H. Mach, R.L. Gill, M. Moszyński, Nucl. Instrum. Methods Phys. Res. A **280**, 49 (1989).
2. E.R. White *et al.*, Phys. Rev. C **76**, 057303 (2007).
3. E.V.D. van Loef, P. Dorenbos, C.W.E. van Eijk, K.W. Krämer, H.U. Güdel, Appl. Phys. Lett. **79**, 1573 (2001).
4. E.V.D. van Loef, P. Dorenbos, C.W.E. van Eijk, K.W. Krämer, H.U. Güdel, Nucl. Instrum. Methods Phys. Res. A **486**, 254 (2002).
5. S. Essabaa *et al.*, Nucl. Instrum. Methods Phys. Res. B **204**, 780 (2003).
6. S. Sundell, H.L. Ravn and the ISOLDE Collaboration, Nucl. Instrum. Methods Phys. Res. B **70**, 160 (1992).
7. J. Le Bris *et al.*, Internal Report IPNO 0603 (English version), Rapport interne IPNO 0504 (French version).
8. I. Deloncle, in preparation.
9. I. Deloncle, M.-G. Porquet, M. Dziri-Marce, Nucl. Instrum. Methods Phys. Res. A **357**, 150 (1995).
10. M. Moszyński, H. Mach, Nucl. Instrum. Methods Phys. Res. A **277**, 407 (1989).
11. A.A. Sonzogni, Nucl. Data Sheets **98**, 515 (2003).
12. J. Pouthas, S. Agarwal, M. Engrand, C. Pisani, Nucl. Instrum. Methods **145**, 445 (1977).
13. E. Browne, J.K. Tuli, Nucl. Data Sheets **108**, 2173 (2007).
14. E. Monnand, R. Brissot, J. Crancon, C. Ristori, F. Schussler, A. Moussa, J. Phys. (Paris) **36**, 1 (1975).
15. T.W. Burrows, Nucl. Data Sheets **92**, 623 (2001).
16. E. Achterberg *et al.*, Phys. Rev. C **5**, 1759 (1972).
17. B.H. Wildenthal, E. Newman, R.L. Auble, Phys. Rev. C **3**, 1199 (1971).
18. A. Nowak *et al.*, Eur. Phys. J. A **6**, 1 (1999).
19. S.H. Faller *et al.*, Phys. Rev. C **38**, 905 (1988).
20. D.M. Symochko, E. Browne, J.K. Tuli, Nucl. Data Sheets **110**, 2945 (2009).
21. S. Ohya, Nucl. Data Sheets **111**, 1619 (2010).
22. S. Ohya, Nucl. Data Sheets **102**, 547 (2004).
23. J. Katakura, Nucl. Data Sheets **86**, 955 (1999).
24. K. Kitao, M. Oshima, Nucl. Data Sheets **77**, 1 (1996).
25. Y. Tendow, Nucl. Data Sheets **77**, 631 (1996).
26. Yu. Khazov, I. Mitropolsky, A. Rodionov, Nucl. Data Sheets **107**, 2715 (2006).
27. S. Rab, Nucl. Data Sheets **75**, 491 (1995).
28. B. Singh, A.A. Rodionov, Yu.L. Khazov, Nucl. Data Sheets **109**, 517 (2008).
29. J.K. Tuli, D.F. Winchell, Nucl. Data Sheets **92**, 277 (2001).
30. J.K. Tuli, Nucl. Data Sheets **94**, 605 (2001).
31. E. Browne, J.K. Tuli, Nucl. Data Sheets **110**, 507 (2009).
32. N. Nica, Nucl. Data Sheets **110**, 749 (2009).
33. B. Singh, Nucl. Data Sheets **102**, 1 (2004).
34. B. Singh, Nucl. Data Sheets **110**, 1 (2009).
35. R.G. Helmer, Nucl. Data Sheets **107**, 507 (2006).
36. D.C. Choudhury, J.N. Friedman, Phys. Rev. C **3**, 1619 (1971).
37. S.H. Liu *et al.*, Phys. Rev. C **80**, 044314 (2009).